Tendon response to matrix unloading is determined by the patho-physiological niche

Wunderli, Stefania L ; Blache, Ulrich ; Beretta Piccoli, Agnese ; Niederöst, Barbara ; Holenstein, Claude N ; Passini, Fabian S ; Silván, Unai ; Bundgaard, Louise ; Auf dem Keller, Ulrich ; Snedeker, Jess G

Abstract: Although the molecular mechanisms behind tendon disease remain obscure, aberrant stromal matrix turnover and tissue hypervascularity are known hallmarks of advanced tendinopathy. We harness a tendon explant model to unwind complex cross-talk between the stromal and vascular tissue compartments. We identify the hypervascular tendon niche as a state-switch that gates degenerative matrix remodeling within the tissue stroma. Here pathological conditions resembling hypervascular tendon disease provoke rapid cell-mediated tissue breakdown upon mechanical unloading, in contrast to unloaded tendons that remain functionally stable in physiological low-oxygen/-temperature niches. Analyses of the stromal tissue transcriptome and secretome reveal that a stromal niche with elevated tissue oxygenation and temperature drives a ROS mediated cellular stress response that leads to adoption of an immune-modulatory phenotype within the degrading stromal tissue. Degradomic analysis further reveals a surprisingly rich set of active matrix proteases behind the progressive loss of tissue mechanics. We conclude that the tendon stromal compartment responds to aberrant mechanical unloading in a manner that is highly dependent on the vascular niche, with ROS gating a complex proteolytic breakdown of the functional collagen backbone.

DOI: https://doi.org/10.1016/j.matbio.2019.12.003

Tendon response to matrix unloading is determined by the patho-physiological niche

Stefania L. Wunderli[a,b], Ulrich Blache[a,b], Agnese Beretta Piccoli[a,b], Barbara Niederöst[a,b], Claude N. Holenstein[a,b], Fabian S. Passini[a,b], Unai Silván[a,b], Louise Bundgaard[c], Ulrich auf dem Keller[c] and Jess G. Snedeker[a,b]

***a* - University Hospital Balgrist,** *University of Zurich, Switzerland*
***b* - Institute for Biomechanics,** *ETH Zurich, Switzerland*
***c* - Department of Biotechnology and Biomedicine,** *Technical University of Denmark, Denmark*

Correspondence to Jess G. Snedeker: *Balgrist Campus, Lengghalde 5, CH - 8008, Zürich, Switzerland.*
jess.snedeker@hest.ethz.ch.
https://doi.org/10.1016/j.matbio.2019.12.003

Abstract

Although the molecular mechanisms behind tendon disease remain obscure, aberrant stromal matrix turnover and tissue hypervascularity are known hallmarks of advanced tendinopathy. We harness a tendon explant model to unwind complex cross-talk between the stromal and vascular tissue compartments. We identify the hypervascular tendon niche as a state-switch that gates degenerative matrix remodeling within the tissue stroma. Here pathological conditions resembling hypervascular tendon disease provoke rapid cell-mediated tissue breakdown upon mechanical unloading, in contrast to unloaded tendons that remain functionally stable in physiological low-oxygen/-temperature niches. Analyses of the stromal tissue transcriptome and secretome reveal that a stromal niche with elevated tissue oxygenation and temperature drives a ROS mediated cellular stress response that leads to adoption of an immune-modulatory phenotype within the degrading stromal tissue. Degradomic analysis further reveals a surprisingly rich set of active matrix proteases behind the progressive loss of tissue mechanics. We conclude that the tendon stromal compartment responds to aberrant mechanical unloading in a manner that is highly dependent on the vascular niche, with ROS gating a complex proteolytic breakdown of the functional collagen backbone.

Introduction

Tendon is a highly specialized connective tissue that consists of sparsely distributed stromal tendon fibroblasts in a collagen-rich extracellular matrix (ECM). The tightly packed and highly structured tendon ECM reflects its capacity to bear physiologically extreme mechanical stresses. The load bearing tendon core comprises hierarchically organized type-I collagen fibrils, fibers and fascicles (or fiber bundles) [1], with fascicles representing a basic physiological unit of the stromal tissue [2]. Biological and mechanical signals are understood to regulate the lifelong adaption of tendon tissue to individual functional demands, with the tissue balanced at the edge of mechanical homeostasis [3]. This delicate balance is often lost, leading to tendon disorders that account for 30−50% of all musculoskeletal clinical complaints associated with pain [4].

Our understanding of the molecular and cellular mechanisms behind tendon physiology and pathology is limited. The severity of tendon pathology is typically graded by histopathological scoring that characterizes the extent of disorganized collagen matrix, abnormal cell shape, presence of inflammation, increased cellularity, tissue vascularity and neuronal ingrowth [5]. These hallmarks of disease intimately involve tissue turnover and proteolytic breakdown of the ECM [6,7]. However, the molecular initiation and regulation of disease related tissue

catabolism within the stromal tendon core remains obscure.

It has long been known that *in vitro* tendon tissue breakdown occurs upon load-deprivation of explants in standard culture conditions (pO_2 20 kPa, 10% serum) [8]. Although almost universally ignored, it is important to note that these culture conditions represent a patho-physiological *in vivo* state in terms of tendon nutrient and oxygen availability, as healthy tendons are only minimally vascularized and minimally oxygenated [9–11]. Tendon fibroblasts normally reside in a state of relative metabolic quiescence under physiological conditions [12]. Tendon repair thus likely involves closely coordinated interaction between the quiescent, avascular intrinsic tendon core compartment and an extrinsic synovial compartment of the tissue that connects to the vascular, immune and nervous systems (Fig. 1A) [13]. Patho-histological investigations confirm the widely accepted clinical paradigm that a presence of blood vessels within the tendon core clearly indicates advanced tissue disease, however the biological consequences of tissue hypervascularity are relatively unexplored [14]. We thus set out to determine if and how such extrinsic factors govern pathological processes in stromal cells of the intrinsic compartment. We established an *ex vivo* system in which tissue culture conditions represent the extrinsic-niche with explanted murine tail tendon fascicles considered as an independent unit of the intrinsic stromal compartment (Fig. 1B).

In this study we investigated how deviations from a tissue niche with physiological temperature and oxygen availability affect resident stromal cells. We

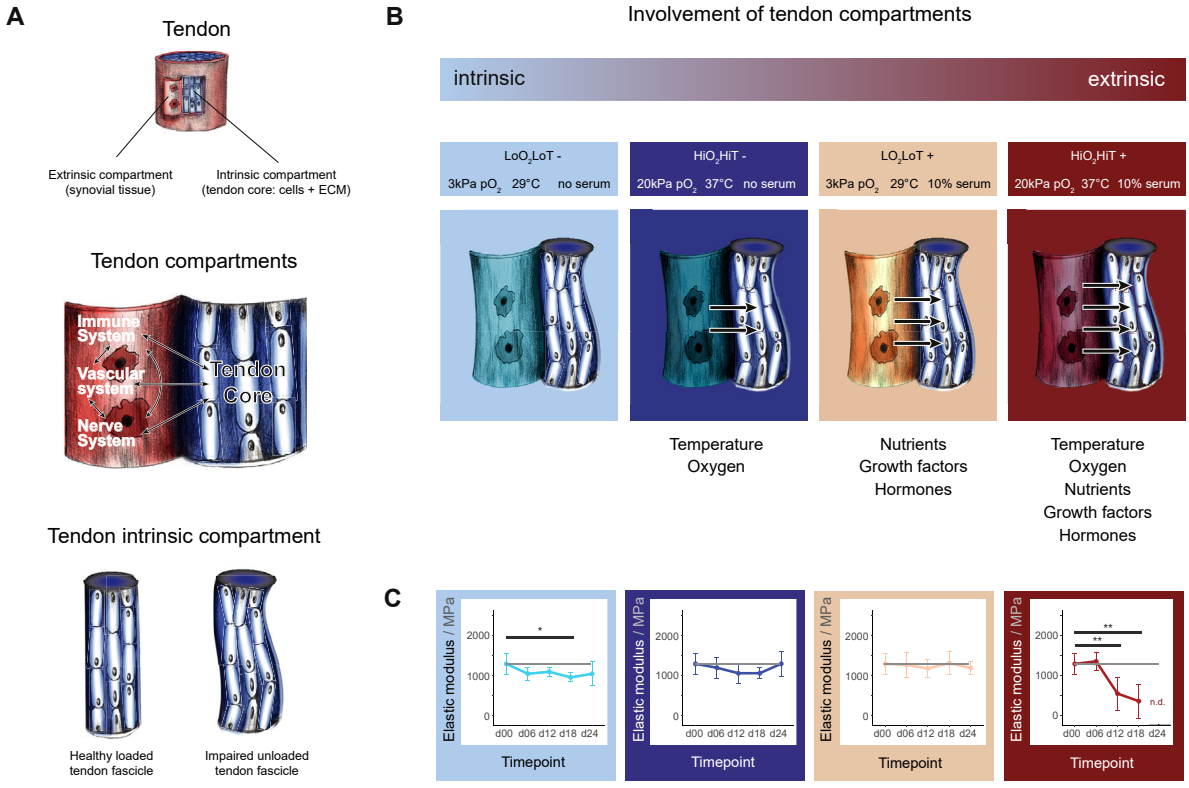

Fig. 1. Tendon compartments, study conceptualization and tendon functional (mechanical) properties. (**A**) The tendon consists of an intrinsic and an extrinsic compartment that likely interact to properly maintain the tissue. The extrinsic compartment comprises a synovium-like wrapping layer that connects the immune, vascular and nervous systems. The intrinsic compartment represents the tendon core and is composed of ECM and cells. The tendon fascicle is the basic functional unit of the tendon and contains ECM and cells of the tendon core. In a healthy homeostatic tissue tendon fascicles are tensioned by intrinsic cellular forces and extrinsic muscle loads. Unloading of tendon fascicles may occur due to overloading and subsequent rupture of sub-tissue structures or upon immobilization. (**B**) The study used unloaded murine tail tendon fascicle as an *ex vivo* model of the damaged tendon core. By varying temperature, oxygen and serum content of the culture conditions we mimicked the degree of involvement of the extrinsic compartment on the cell-driven remodeling process. (**C**) Elastic moduli of tendon fascicles cultured in different mimicked niches over 24 days (d24). The data points represent mean values with error bars representing standard deviations. Statistical analysis was performed using one-way ANOVA followed by contrast analysis in RStudio. Mean values at each time-point (d06 – d24) were compared to the freshly isolated control (d00) within each condition (N = 6, p-values: * < 0.05, ** < 0.01).

specifically hypothesized that the tissue niche is an important regulator of proteolytic cellular response to matrix damage. We compared mechanical properties, cell viability, metabolic activity, tissue morphology, whole transcriptomes, and protein degradomes and secretomes. We were able to identify mechanisms of extrinsic tendon compartment regulation of intrinsic tendon cells. We observed a vascular state-dependent switch from tissue homeostasis to pathologic tissue degeneration that was mediated by activation of immune-related cellular responses, production of reactive oxygen species and downstream activation of proteolytic enzymes.

Results

Mechanical degradation of load-deprived tendon fascicles is greatly accelerated in *ex vivo* culture conditions that mimic a hypervascularized stromal niche

We established a tendon explant model to investigate the impact of extrinsic tissue factors on underload-induced alterations in tendon core mechanical properties. Intact tendon fascicles were isolated from murine tails and cultured while being deprived from load to mimic tendon underloading after damage or immobilization. Tendon fascicles were cultured with or without serum and under varying temperature and oxygen levels to study the involvement of extrinsic factors associated with vascularization under tightly controlled conditions (Fig. 1B). Fascicles were cultured in serum-free medium, at low oxygen partial pressure (3 kPa pO_2) and low temperature (29 °C) to mimic a quiescent, minimally nourished tissue that is typical of the tendon core within a healthy tissue [10,11] (Supplementary fig. S1). In contrast, a pathologically vascularized tissue was mimicked by elevated temperature, oxygen and nutrients (37 °C, 20 kPa pO_2, 10% serum) that would follow upon ingrowth of blood vessels and synovial tissue.

High tensile strength and high elastic modulus characterize functional tendon tissue that has been optimized for transmission of muscle forces across joints of the body. To evaluate the effect of tissue culture niche on tendon mechanical integrity we measured the elastic moduli of tendon fascicles after 6, 12, 18 and 24 days (d06 − d24). Elastic moduli were calculated from force-displacement curves recorded on a custom-made uniaxial test device [15]. The elastic modulus of freshly isolated (uncultured) fascicles was 1300 MPa (sd: 242 MPa). Load-deprivation did not affect elastic moduli of tissues in serum-free conditions at all tested temperatures and tissue oxygenation levels, with the tissue remaining functionally stable throughout the experimental period (Fig. 1C). Tissues remained similarly stable when including serum to the low temperature (29 °C) and low oxygen (3 kPa pO_2) conditions (Fig. 1C). In contrast, the combination of serum, high temperature, and high oxygen (10% serum, 37 °C, 20 kPa pO_2) strongly and significantly decreased the elastic modulus in these conditions mimicking a pathologically vascularized tendon niche (Fig. 1C). Onset of diminished elastic modulus was detectable at day 12 and dropped to 367 MPa (sd: 426 MPa) at day 18. At day 24 it was no longer possible to measure the elastic modulus due to a complete loss of load bearing capacity. Notably, the decrease of mechanical properties did not occur in devitalized control tendons, indicating that intrinsic cellular processes and not proteolytic activity of serum components were responsible for tissue degradation (Supplementary fig. S2).

Oxygen- and temperature-dependent losses of mechanical properties in serum-containing cultures was additive, with low oxygen (37 °C, 3 kPa pO_2) and low temperature (29 °C, 20 kPa pO_2) each slowing the rate of mechanical degradation (Supplementary fig. S3). Multiple linear regression analysis of culture time-point, temperature, serum and oxygen revealed a significant regression equation ($F(6, 127)$, 5.494, $p = 4.37 \times 10^{-5}$) with an R^2 of 0.21. The regression model significantly predicted elastic modulus with culture time-point being determinant (β of d12 $= -200.1$, $p = 0.02$, β of d18 $= -195.8$, $p = 6.2 \times 10^{-4}$, β of d24 $= -255.4$, $p = 6.3 \times 10^{-3}$), as well as temperature ($\beta = -284.5$, $p = 2.89 \times 10^{-5}$) and oxygen ($\beta = 163.26$, $p = 0.013$). Surprisingly, presence of serum was not a significant predictor ($\beta = -49.15$, $p < 0.45$).

In summary, we established a novel *ex vivo* tendon model that represents different levels of extrinsic compartment involvement during underload-mediated tendon remodeling. Experiments revealed that cell-mediated processes drive loss of mechanical properties of the tendon fascicles at activating *ex vivo* conditions (high levels of oxygen and temperature).

Comparable cell viability, metabolism and collagen fiber continuity in functionally impaired and intact tendon fascicles

We next aimed to clarify how load-deprivation, high temperature and oxygen combine to drive tissue breakdown. We first verified that passive thermodynamic effects related to proteolytic kinetics were not responsible for the observed acceleration of tissue degradation at higher culture temperatures [16] (Supplementary fig. S3). We then focused on comparisons of cellular responses in niches mimicking low tissue vascularity (LoO_2LoT) and high tissue vascularity (HiO_2HiT), seeking to understand how

the mimicked vascular niche led to the observed loss of mechanical function.

To evaluate whether cell number or viability contributed to altered mechanical properties we performed a fluorescence-based cell viability assay in tendon fascicles after 6, 12, 18 and 24 days of culture. Total cell number and cell viability within the tissue were not markedly different between the two conditions (Fig. 2A). Metabolic activity as measured by ATP concentration increased at all time points, indicating a switch from a more quiescent to a more active cellular state in all tested conditions when compared to the freshly isolated d00 controls (Supplementary fig. S4). To investigate tendon fascicle morphology, we looked at macroscopic alterations and additionally performed second harmonic generation imaging of collagen fiber structure. In both conditions, fascicles showed length contraction over time with apparently intact collagen fibers (Fig. 2B(2)). Contraction of fascicles in the HiO_2-HiT + conditions was more pronounced with a less compact morphology compared to the LoO_2-LoT+ group. The ultra-structure of collagen fibrils was also comparable between both groups as revealed by transmission electron microscopy (Fig. 2B(3), (4)).

Taken together, our data show that the loss of mechanical properties correlates with only minor morphological changes at the cell and tissue matrix levels. We next aimed at investigating changes that take place at the molecular level.

Mechanical impairment is associated with strong transcriptome changes related to immune system response, oxidative-stress, lysosome activation and proteolysis

To investigate the molecular changes that are involved in the loss of mechanical properties we compared conditions yielding functionally impaired (HiO_2HiT+) and intact (LoO_2LoT+) tendon fascicles by transcriptome analysis using RNA sequencing (RNA-seq). Overall, we detected 23'675 known transcripts according to the murine reference genome. Filtering revealed 3305 differentially expressed genes (DEG) between the two groups, among which 1'854 were up-regulated and 1'451 were down-regulated in the functionally impaired fascicles

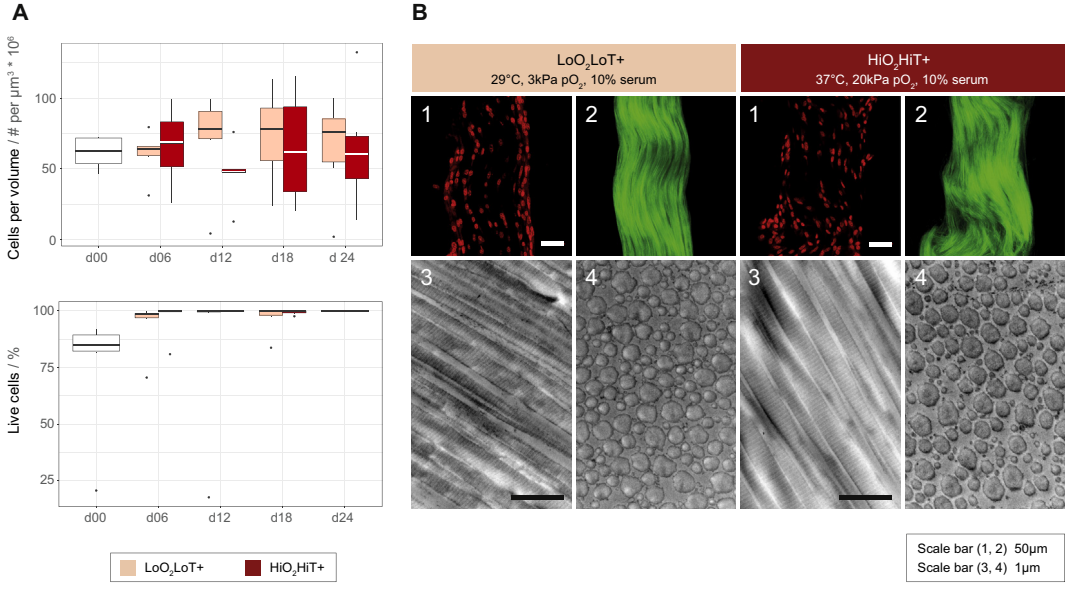

Fig. 2. Cell viability and morphological characterization of mechanically intact and impaired tendon fascicles. (**A**) Total cell number per volume (upper) stayed constant over time and cell viability (lower) was not significantly different between the HiO_2HiT+ and the LoO_2LoT+ group at any time-point. Isolated regions of dead cells on the periphery were always present in the d00 condition, most probably due to the process of physical tissue extraction. However, these cells disappeared upon culture in serum, which explains the slightly lower percentage of live cells in the d00 condition. Boxplots display median values and 1st/3rd quartiles. Outliers are plotted as individual data points. Statistical analysis was performed using Mann-Whitney *U* test in RStudio comparing the LoO_2LoT+ to the HiO_2HiT+ condition within each time point (d06 − d24) (N = 6). (**B**) Tissue morphology after a treatment period of 12 days. (1) Second harmonic generation imaging and (2) nuclear shape of mouse tail tendon fascicles treated at either low oxygen and low temperature with serum (LoO_2LoT+) or high oxygen and high temperature with serum (HiO_2HiT+). (3) Transmission electron microscopy images in longitudinal and (4) transverse sections. Scale bars represent 50 µm in the upper fluorescence images and 1 µm in the electron micrographs.

(Fig. 3A and supplementary Table ST1). Interestingly, only 173 genes belong to the matrisome (as highlighted in supplementary Table ST1 according to the MatrisomeDB [17]), of which 25% are assigned to the core matrisome and 75% to matrisome-associated genes (Supplementary Fig. 5A). To systematically investigate the relationship between all DEGs, we functionally enriched them within the gene ontology (GO) "Biological Process". Over-represented GO terms included inflammatory response, immune-related processes, signal transduction (e.g. G-protein coupled receptor signaling) and response to phagocytosis (see Supplementary Table ST2 "both"). Of these overrepresented terms, nearly 50% were also found when considering only up-regulated genes (Supplementary Table ST2 "up"). All DEGs were further mapped to the most relevant pathways via statistical enrichment analysis using the MetaCore database (Fig. 3B).

Strikingly, 7 out of 10 pathways are related to immune system activation including professional phagocytic cells, such as neutrophils, macrophages and dendritic cells. In addition, three identified pathways ("Chemokines in inflammation", "HIF-1 target transcription" and "Activation of NADPH oxidase") are closely linked to oxidative-stress-dependent processes (Fig. 3B). The induced oxidative-stress related genes mainly include regulatory proteins or subunits of the NADPH oxidase (Nox2/Cybb/gp91phox, Cyba/p22phox, Ncf1/p47phox, Ncf2/p67phox, Ncf4/p40phox, Rac2, Vav1, Vav3), a transmembrane protein that catalyzes the production of superoxide in different cell types (Supplementary fig. S5B). All of these genes were significantly up-regulated in the HiO_2HiT+ group.

Alternately we enriched all DEGs in the Kyoto Encyclopedia of Genes and Genomes (KEGG) domain. One half of the top 10 identified gene pathways is associated with inward vesicular trafficking destined to degradation in the lysosome ("Lysosomes", "Phagosomes", "Fc gamma R-mediated phagocytosis", "*Staphylococcus aureus* infection", "NOD-like receptor signaling pathway") (Fig. 3B). The lysosome is the main catabolic subcellular organelle responsible for degradation of extracellular and intracellular components. Furthermore, "Osteoclast differentiation" suggests initiation of a process that is relevant in ECM resorption as shown by up-regulation of the genes *Pparg*, *Csf1*, *Pi3k*, *Tnfrsf11A* (*Rank*) and *Tnfsf11* (*Rankl*) and others (Supplementary fig. S5C). The KEGG pathway analysis including only up-regulated DEGs is mostly consistent with the analysis including both, up- and down-regulated genes (Fig. 3B, Supplementary fig. S5D).

Because we previously showed that tendon fascicles in the HiO_2HiT+ condition lose mechanical properties by processes that most likely involves ECM breakdown, combined with pathway analysis of DEGs suggesting lysosomal degradation as a central process, we examined the GO term "proteolysis" (GO:0006508). Indeed 96 DEGs were annotated to "proteolysis", of which 67 were up-regulated in the vascular niche mimicking condition (HiO_2HiT+) (Fig. 3C). Involved DEGs included extracellular proteases such as matrix metalloproteinases (*Mmp8, 9, 10, 13, 27*), a disintegrin and metalloproteinases (with thrombospondin motifs) (*Adam 3, 8, 17, 23, 32* and *Adamts 15, 16, 17, 19, 20*), intracellular proteases involved in lysosomal degradation such as cathepsins (*Ctsa, Ctsb, Ctsc, Ctsd, Ctsf, Ctso, Ctss, Ctsz*) and proteasome-related proteins (*Psma8*, *Psmb3, 8, 9*).

In summary, the data reveal transcriptome changes between the conditions mimicking a minimally-vascularized niche (LoO_2LoT+) and hypervascular mimicking conditions that lead to matrix breakdown (HiO_2HiT+). The changes heavily involve pathways related to proteolysis, oxidative-stress-related processes, immune system activation and lysosome involvement. Up-regulation of these pathways was accompanied by and well-explain, the observed functional loss of fascicle mechanics in culture conditions containing serum, high oxygen, and high temperature.

Tendon mechanical integrity is rescued by inhibiting reactive oxygen species and proteases

Based on the experimental design (difference in temperature and oxygen saturation between the two groups) and the noted up-regulation of oxidative stress-related pathways, we hypothesized that reactive oxygen species (ROS) regulate ECM degradation and loss of tendon mechanical integrity. To confirm ROS production we measured fluorescence of dichlorofluorescein (DCF). ROS were significantly increased in conditions leading to functionally impaired fascicles (HiO_2HiT+) compared to the intact tissues (LoO_2LoT+), confirming the RNA-seq findings on the tissue level (Supplementary fig. S6).

Based on our RNA-seq data we hypothesized that ROS and MMPs are involved in tendon fascicle degeneration. We therefore assessed the effects of ROS scavenging (Tempol) and broad spectrum MMP inhibition (Ilomastat) in the conditions leading to functional impairment (HiO_2HiT+) over a time period of 12 days. Separate inhibition of ROS and MMPs both partially protected against loss of mechanical properties as measured by the elastic moduli (Fig. 4A). Combined inhibition of both ROS and MMPs remarkably resulted in complete maintenance of elastic modulus at levels comparable to freshly isolated control fascicles. A passive chemical cross-linking effect of the inhibitory substances could be excluded by control experiments on devitalized

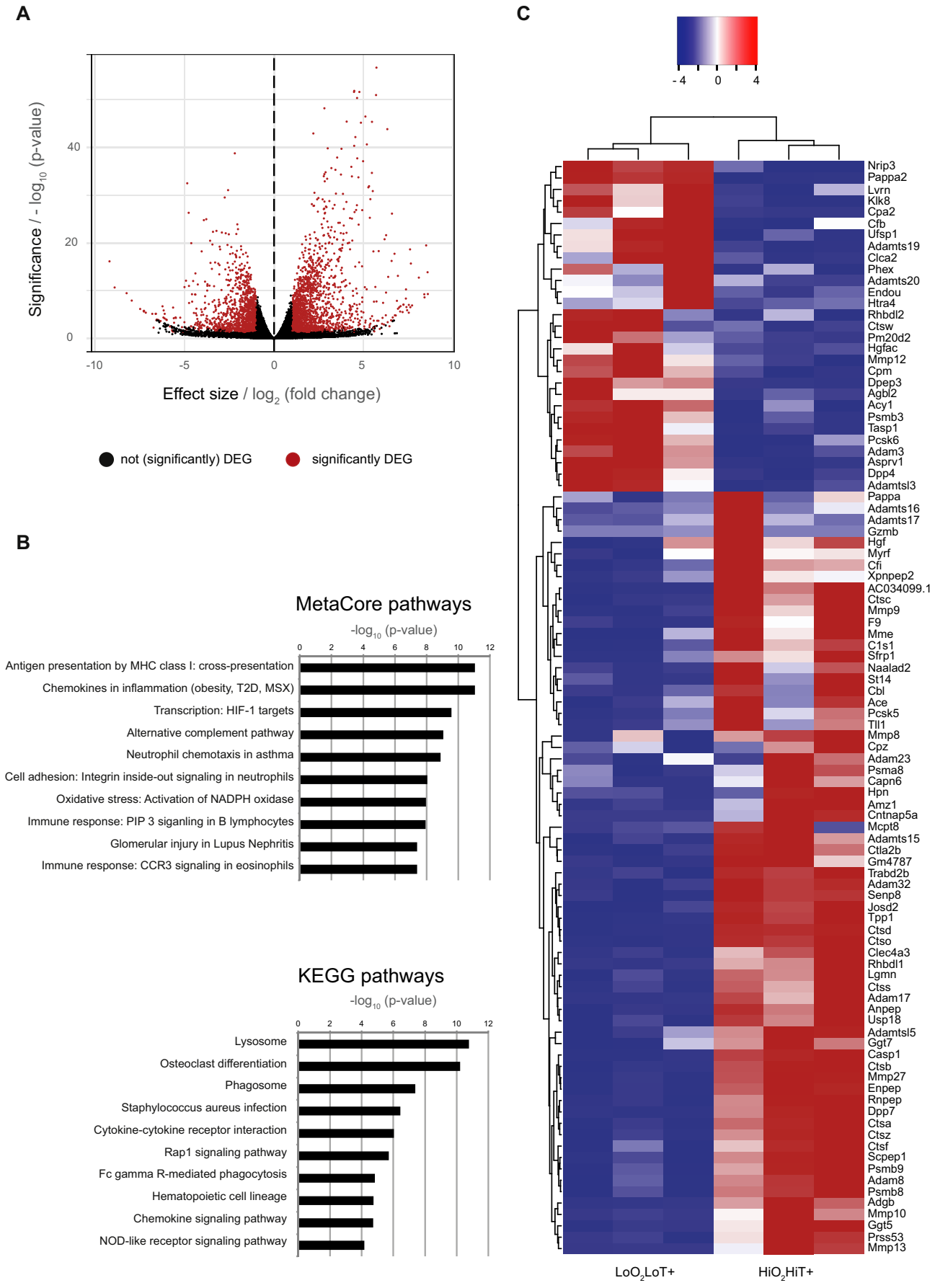
A
Significance / - log10 (p-value)
40
20
0
-10
-5
0
5
10
Effect size / log2 (fold change)
not (significantly) DEG
significantly DEG
B
MetaCore pathways
-log10 (p-value)
0 2 4 6 8 10 12
Antigen presentation by MHC class I: cross-presentation
Chemokines in inflammation (obesity, T2D, MSX)
Transcription: HIF-1 targets
Alternative complement pathway
Neutrophil chemotaxis in asthma
Cell adhesion: Integrin inside-out signaling in neutrophils
Oxidative stress: Activation of NADPH oxidase
Immune response: PIP 3 siganling in B lymphocytes
Glomerular injury in Lupus Nephritis
Immune response: CCR3 signaling in eosinophils
KEGG pathways
-log10 (p-value)
0 2 4 6 8 10 12
Lysosome
Osteoclast differentiation
Phagosome
Staphylococcus aureus infection
Cytokine-cytokine receptor interaction
Rap1 signaling pathway
Fc gamma R-mediated phagocytosis
Hematopoietic cell lineage
Chemokine signaling pathway
NOD-like receptor signaling pathway
C
- 4
0
4
Nrip3
Pappa2
Lvrn
Klk8
Cpa2
Cfb
Ufsp1
Adamts19
Clca2
Phex
Adamts20
Endou
Htra4
Rhbdl2
Ctsw
Pm20d2
Hgfac
Mmp12
Cpm
Dpep3
Agbl2
Acy1
Psmb3
Tasp1
Pcsk6
Adam3
Asprv1
Dpp4
Adamtsl3
Pappa
Adamts16
Adamts17
Gzmb
Hgf
Myrf
Cfi
Xpnpep2
AC034099.1
Ctsc
Mmp9
F9
Mme
C1s1
Sfrp1
Naalad2
St14
Cbl
Ace
Pcsk5
Tll1
Mmp8
Cpz
Adam23
Psma8
Capn6
Hpn
Amz1
Cntnap5a
Mcpt8
Adamts15
Ctla2b
Gm4787
Trabd2b
Adam32
Senp8
Josd2
Tpp1
Ctsd
Ctso
Clec4a3
Rhbdl1
Lgmn
Ctss
Adam17
Anpep
Usp18
Adamtsl5
Ggt7
Casp1
Ctsb
Mmp27
Enpep
Rnpep
Dpp7
Ctsa
Ctsz
Ctsf
Scpep1
Psmb9
Adam8
Psmb8
Adgb
Mmp10
Ggt5
Prss53
Mmp13
LoO2LoT+
HiO2HiT+

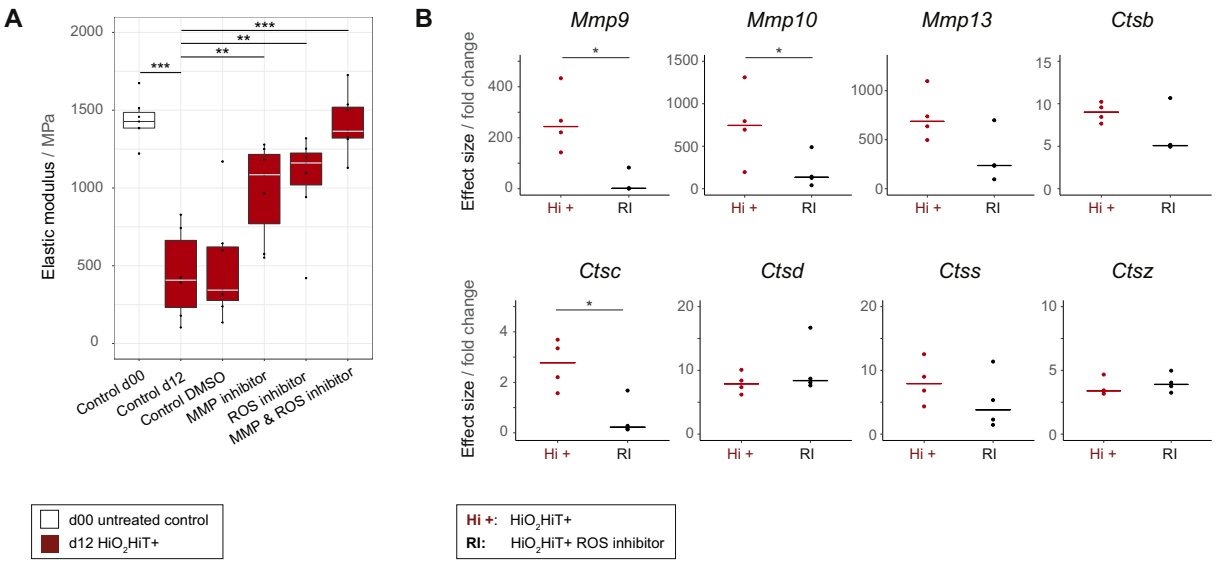

Fig. 4. Inhibition of reactive oxygen species (ROS) and matrix metalloproteinases (MMPs) in mechanically impaired tendons. (**A**) Inhibition of ROS and MMPs by Tempol and Ilomastat, respectively. Culture of 12 days with inhibition of ROS or MMP results in preserved elastic modulus compared to the control group. Inhibition of ROS and MMPs show an additive effect in preserving mechanical properties (Control d00). Boxplots display median values and 1st/3rd quartiles. Outliers are plotted as individual data points. Statistical analysis was performed using one-way ANOVA followed by contrast analysis in RStudio. Mean values of groups treated with inhibitory substances were compared to the control group cultured for 12 days in serum-supplemented medium (Control d12) (N = 6). (**B**) RT-PCR gene expression of proteins involved in ECM remodeling after 12 days of culture with and without the ROS inhibitor Tempol (N = 4). *Mmp9*, *Mmp10* and cathepsin C (*Ctsc*) were significantly down-regulated (p-value = 0.029 for all) in tendon tissue by inhibiting ROS. Gene expression of *Mmp13* and cathepsins B, D, S and Z (*Ctsb, Ctsd, Ctss, Ctsz*) was not significantly affected by ROS inhibition. However, a trend of regulation towards native gene expression is observed in *Mmp13* and *Ctsb* and *Ctss*. Displayed are the relative fold changes compared to the freshly isolated control at day 0 and the horizontal crossbar represents the median. All values were normalized to the reference gene (*Anxa5*). Mann-Whitney U tests were performed using in RStudio by comparing the Tempol-supplemented group to the HiO_2HiT+ group (N = 4, p-values: * < 0.05, ** < 0.01, *** < 0.001).

tendon tissue samples (Supplementary fig. S7A). Based on the observed additive effect of blocking ROS and MMPs we hypothesized that ROS and MMPs may be hierarchically linked. To address this hypothesis, we performed RT-PCR on fascicles cultured in the HiO_2HiT + environment with or without Tempol inhibition of ROS. We examined eight genes of interest that had been previously related to proteolysis in our RNA-seq results (*Mmp9, Mmp10* and *Mmp13*, *Ctsb*, *Ctsc*, *Ctsd*, *Ctss* and *Ctsz*). Gene expression of *Mmp9*, *Mmp10* and *Ctsc* was significantly down-regulated by inhibiting ROS with Tempol after 12 days (Fig. 4B, supplementary fig. S7B). A trend towards lower expression of *Mmp13*, *Ctsb* and *Ctss* was observed too. Expression of *Ctsd* and *Ctsz* was not affected by inhibition of ROS. These data show that ROS regulate matrix metalloproteinase and cathepsin gene expression directly or indirectly through factors up-stream of nuclear transcription of these proteases.

Taken together, our findings suggest that elevated oxygen and temperature act as pathological drivers of fibroblast activation in the tendon core. These cells undergo multifactorial molecular processes that

Fig. 3. Transcriptome analysis of differentially expressed genes (DEG) in mechanically intact vs. impaired tendon fascicles. (**A**) Volcano plot of differentially expressed genes between tendon fascicles cultured in HiO_2HiT+ and LoO_2LoT+. Genes colored in red are considered as differentially expressed with a |fold change| > 2 and a significance of $p < 0.05$. (**B**) The top 10 enriched signaling pathways in the HiO_2HiT + group compared to the LoO_2LoT+ group (determined according to the lowest p-values obtained from the MetaCore and KEGG database using both, up- and down-regulated genes). MHC = Major Histocompatibility Complex, T2D = Type 2 Diabetes, MSX = Metabolic Syndrome X (**C**) Unsupervised hierarchical clustering of DEG belonging to the GO term "proteolysis" (GO:0006508) in the intact LoO_2LoT+ and the degrading HiO_2HiT + group. Each column represents one biological replicate (N = 3 per group). Depicted are the DEGs with cut-off values of |fold change| > 2 and $p < 0.05$. The clustering separates the genes by color with positive or negative row-scaled Z-scores represented in red and blue, respectively. (For interpretation of the references to color in this figure legend, the reader is referred to the Web version of this article.)

involve oxidative-stress and immune system activation pathways. Inhibiting these pathways was sufficient to abrogate ECM degradation and functional impairment in unloaded tendon explants.

Tendon degradome shows niche dependent activity of matrix metalloproteinases and lysosomal proteases

To quantify proteins and N-termini and thereby identify proteolytic cleavage events in intact and degraded tendon explants, we performed 10plex-Tandem Mass Tag™-Terminal amine isotopic labeling of substrates (TMT-TAILS) (Fig. 5A). 382 proteins were quantified with high confidence (FDR < 0.01), of which 35 were significantly more and 13 significantly less (adj. p-value < 0.05; |fold change| > 1.5) abundant in the degraded HiO_2-HiT + phenotype group (Fig. 5B, Supplementary Table ST3). More abundant hits included proteins associated with proteolysis or lysosomes (MMP3, MMP13, beta-glucuronidase BGLR, lysosomal protective protein/cathepsin A CTSA, cathepsin Z CTSZ, V-type proton ATPase subunits VATA, VATE1, VATG1, lysosomal acid phosphatase), intracellular trafficking (sorting nexin 3/5 SNX3, SNX5, programmed cell death 6- interacting protein PDC6I, glycolipid transfer protein GLTP) and ROS metabolism (catalase CATA, peroxiredoxin 1 PRDX1). Less abundant proteins are associated

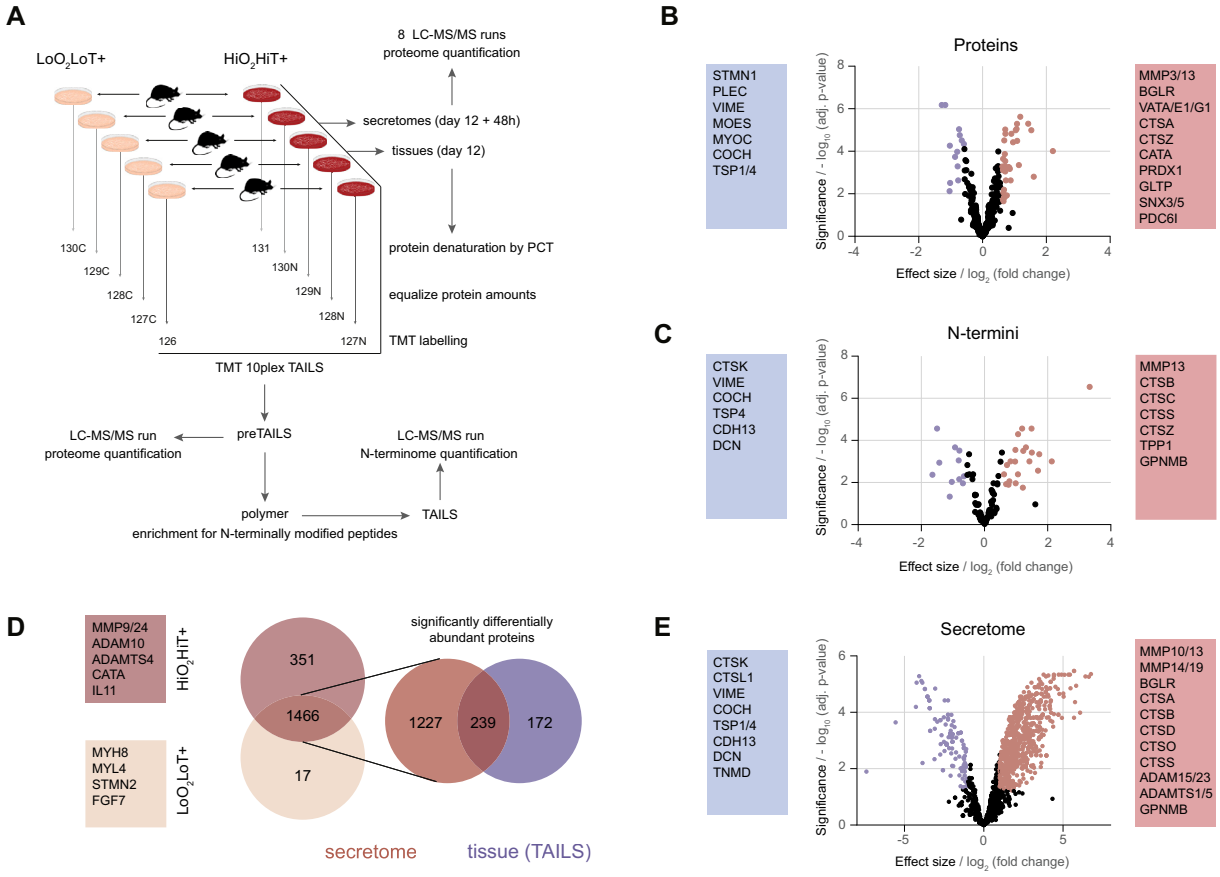

Fig. 5. Proteomic analysis of mechanically intact (LoO_2LoT+) and impaired (HiO_2HiT+) tendon fascicles. (**A**) TMT-TAILS workflow. Tissues of each condition (N = 5) were collected after 12 days. Protein amounts of all tissue samples were equalized and subsequently analyzed in a 10plex TMT-TAILS experiment. Medium for secretome collection (N = 4) was additionally conditioned for 48 h and analyzed by mass spectrometry-based label-free protein quantification method. (**B**) Quantified proteins and (**C**) N termini from TMT-TAILS probes. Proteins colored in red and blue are considered as differentially more or less abundant in the HiO_2HiT+ condition and have significance of $p < 0.05$ and a |fold change| > 1.5 (red) or < 1.5 (blue). (**D**) Venn diagram of quantifiable proteins in the secretomes of the mechanically intact and impaired group. 239 out of totally 1466 secreted proteins were detected both extracellularly (released into the medium) and in the tissue (TAILS experiment). (**E**) Label-free quantification of the 1466 secreted proteins, of which 860 show significantly different abundance. Red dots (740) show significantly more ($p < 0.05$, |fold change| > 2) and blue dots (120) significantly less ($p < 0.05$, |fold change| < 2) abundant proteins in the HiO_2HiT+ group. (For interpretation of the references to color in this figure legend, the reader is referred to the Web version of this article.)

with cytoskeletal organization (vimentin VIME, stathmin STMN1, cochlin COCH, myocilin MYOC, plectin PLEC, moesin MOES) or cell adhesion and ROS production (thrombospondin 1/4 TSP1, TSP4).

Additionally, we extracted 103 N-terminally TMT-labeled N-terminal semi-tryptic quantifiable peptides from 79 different proteins, whereof 46 could be assigned to curated protein start sites and 57 were protease-generated neo-N termini (Fig. 5C, Supplementary Table ST4). Quantitative N-terminome analysis revealed significantly (adj. p-value < 0.05; |fold change| > 1.5) increased abundance of active lysosomal proteases (CTSB, CTSC, CTSS, CTSZ, lysosomal pepstatin-insensitive protease TPP1) all identified by their mature protein N terminus generated upon propeptide removal in the degraded tendon tissue. To our surprise the mature protein N terminus of cathepsin K was inversely abundant in these conditions (elevated in non-degrading niche conditions). Transmembrane glycoprotein NMB (GPNMB), which has been identified in osteoclast and macrophage differentiation, was highly abundant in the degraded phenotype and could be determined by a cleavage site within its extracellular domain. Moreover, N-terminomics corroborated increased abundance of MMP13 in the same group, but by identification of a neo-N-terminal peptide, indicating removal of the hemopexin domain with potential implication in altered substrate specificity. Although below the fold change cut-off of 1.5, we identified 10 collagen type I cleavage sites, of which 8 were significantly more abundant in the mechanically degrading group. Four of these cleavage products were associated with the collagen type I alpha 1 chain (COL1A1) including a known MMP13 site and four with the alpha 2 chain (COL1A2).

We then quantitatively compared proteins released into supernatants of *ex vivo* tendon cultures under degrading and non-degrading conditions. We identified a total number of 2017 proteins with high confidence (FDR < 0.01) (Supplementary Table ST5), of which 351 were only found in the supernatants of the HiO_2HiT+ group (quantifiable in at least two replicates) (e.g. CATA, many proteasome subunit proteins PSMA2, PSMA5, PSMB3, PSMB8, MMP9 and 24, ADAM10, ADAMTS4, IL11) and 17 only in the LoO_2LoT+ group (e.g. Fibroblast growth factor 7 FGF7, Stathmin 2 STMN2). Differential abundance was calculated from 1466 proteins, of which 226 proteins were identified also in the tissue sample (Fig. 5D). 740 proteins were significantly more abundant (adj. p-value < 0.05; |fold change| > 2) in the secretome of the degraded group, accounting for ~85% of all 860 proteins with significantly differential abundance. Quantification of the released proteins corroborated the protease abundance pattern of the tissue transcriptome showing significantly increased extracellular secretion of proteases, such as CTSA, CTSB, CTSD, CTSL, CTSO, CTSS, MMP9, 10 (Stromelysin-2), 13, 14, 19, 24 and ADAM10, 15, 19, 23 and ADAMTS1, 4, 5 in the degraded group (Fig. 5E), while cathepsin K was significantly less abundant in the supernatants of the HiO_2HiT+ group.

Discussion

The mechanisms of tendon remodeling after injury, or in chronic disease, are poorly understood. Although observational studies have described a recruitment of cells from the extrinsic tissue compartments (blood vessels, inflammatory mediators) to the tendon core in diseased tissues [14], the nature of the tissue crosstalk that underlies this recruitment is unknown [18]. The interplay between tendon fibroblasts in the tendon core and extrinsic peritendinous support tissues is complex and remains largely undescribed, mainly because *in vivo* experiments cannot isolate or control extrinsic influences on intrinsic tissues. In this work we studied how the tendon core responds to mechanical load deprivation with an explant model that mimics a damage scenario. We used this model to study how stromal tissue response to unloading is mediated by a niche designed to mimic vascularized tissue.

The fascicle *ex vivo* explant is uniquely suited for study of stromal tissue biology as it maintains the cells in their native tissue microenvironment, provides normal cell-cell and cell-matrix communication, and allows controlled parametric study of cell-mediated matrix turnover in pathophysiological contexts [19–21]. Exploiting this model, we confirmed that standard tissue culture conditions initiate stromal compartment remodeling [8]. Mechanical tension is dogmatically considered as essential to protect tendon tissue from proteolytic turnover and tissue remodeling [22]. However, we highlight the physiological role of low oxygen and below body core temperatures as important in maintaining cellular quiescence and functional integrity of the tendon fascicle ECM. Among other implications, our findings suggest that tendon cell and tissue culture conditions should be reconsidered in experimental settings that study healthy tissue. This does not only apply for the tendon field but also for scientific investigations of other stromal tissues with normally low vascularity, such as cartilage, the intervertebral discs and ligaments.

We showed that hyperoxia and hyperthermia serve as dominant extrinsic triggers for a pathological loss of mechanical properties in load-deprived tissue. We consider these conditions to represent a vascularized tendon niche, such as expected after acute injury or in advanced stages of tendon disease. Our molecular studies revealed that the niche gates the onset of catabolic tissue turnover via a ROS-protease axis.

Comparative quantitative degradomic analysis, revealed measurable cleavage of collagen type I in the degraded tissue, consistent with the according loss of macro-mechanical properties. Activation of cathepsins by proteolytic removal of the propeptide and modifications in substrate binding specificity of MMP13 in the degraded phenotype strongly reinforce the transcriptomic analysis, elaborating in detail the widespread elevation of protease expression. The protease profile was broad, including not only MMPs and cathepsins, but also ADAMs and ADAMTs that are known to contribute to tissue degradation [23].

In our study, we observed that ROS are generated upon tissue exposure to supra-physiological oxygen and temperature levels. An increase in ROS scavenging proteins (CATA, PRDX1) and a decrease in ROS producing proteins (TSP1) was observed, potentially indicating the activation of a feedback mechanism that may compensate emergent ROS imbalances [24]. Although ROS have been hypothesized to be involved in tendon diseases their implications on tendon tissue degradation and mechanical function have not been studied [25]. Intriguingly, we found that ROS generation, the induction of matrix proteases and the subsequent tissue degradation leading to loss of tendon function are hierarchically linked. While we can conclude from our data that in tendon ROS lay upstream of protease activation, it remains unknown whether hyperthermia and hyperoxia activate a precursor component in the serum that serves as an ignition switch for parallel or consecutive processes, such as ROS generation, tissue degradation and immune system activation. Early research on muscle suggests that hyperthermia induced by exercise directly causes oxidative stress through ROS generation and changes in the immune system and inflammatory response by increased cytokine production [26]. According to our RNA-seq dataset it is also conceivable that ROS production and subsequent MMP activation occur via NADPH oxidase, an enzyme that is also known to be activated by TSP1 via the organizer subunit $p47^{phox}$ [27]. We identified the *Cybb/Nox2* gene (and several organizer subunits), a member of the NADPH oxidase family, that is widely accepted to have phagocyte-specific tissue expression [28]. Therefore it seems likely that the cells of the tendon fascicles express a phagocytic-like character or those tissue resident macrophages are expanded and activated [29]. This assumption is further strengthened by the identification of different pathways that are associated with phagocytosis and lysosomes. Furthermore, we identified induced pathways and proteins associated with differentiation of osteoclasts, cells closely related to the family of professional phagocytes. Specifically, the upregulated *Ppar* gene, which is involved in osteoclast differentiation processes, was recently shown to induce a lysosome-controlled ECM catabolism [30]. In line with these results, matrix resorption in our degraded tendon model might be accelerated by lysosomal proteases upon release from lysosomal vesicles that fuse with the plasma membrane as cathepsins were found both in tissue proteome and secretome [31]. Interestingly, many cells with a phagocytic character are also the effector cells of the innate immune system thereby acting to enhance inflammation. Likewise, fragments of proteases may also elicit pro-inflammatory signaling [32]. Therefore, it is tempting to speculate that phagocytosed ECM components are cleaved by proteases within the lysosome and the generated fragments may subsequently serve as mediators of inflammation and immune response as so called damage-associated molecular patterns (DAMPs) [33,34].

Taken together, exogenous peptides generated from ECM breakdown after acute loss of mechanical tension in a pathological tissue may be internalized by phagocytosis, processed in the phagolysosome to produce DAMP-like fragments that serve as "antigens", which are finally presented to the immune system via class I MHC (also found induced in our RNA-seq data) in tendon fibroblasts. This process, also known as cross-presentation [35], has been identified as the most significantly regulated pathway in our impaired tendon model.

Among the limitations of the present study is that tendon tissue was used exclusively from male animals. Although sex as a potentially determinant variable in tendon biology is well described for humans [36] the mechanical behavior and biochemical composition of tendons from male and female mice is very similar [37]. More generally, the inherent potential for disparities between human and murine tissues is a limitation. While caution in extrapolating murine data to humans is prudent, a number of genes expressed in tail tendon model we present have been documented to be also elevated in ruptured human tendons (e.g. *Mmp9, 13, 14, 19, Ctss, Adam 8, 17* and *Adamts 4*) [38–40], with some exceptions (e.g. *Ctsk, Ctsl*) [41]. Unbiased studies on ruptured and mechanically degenerated human tissues are urgently required in this regard. Beyond standard limitations of the model, the experimental approach we adopt only captures unidirectional extrinsic gating of the intrinsic compartment, while neglecting bidirectional signaling between the intrinsic and extrinsic tissue compartments. Such bidirectional signaling between tissue compartments may play a key role in several aspects of tendon tissue physiology, not least of which is how the tissue immune compartment mediates tissue response to injury [42].

In summary, we have developed and deeply characterized a tendon explant model of tissue degeneration to decipher tissue crosstalk between the stromal collagen backbone and its vascular niche.

Our data reveal that tissue temperature and oxygen levels represent decisive contextual cues that trigger ECM proteolysis. These data yield central insights into the activation of initially quiescent tendon cells to work as executers of pathological tissue remodeling.

Experimental procedures

Ex vivo tissue culture

Tendon fascicles were extracted from tails of freshly euthanized 12−13 weeks old wild-type C57BL6/J male mice. Tendon fascicles were gently isolated from each tail using a surgical clamp and distributed among the control and treatment groups in a non-biased fashion. The explanted fascicles were cultivated in absence of mechanical load and examined at designated time-points (6, 12, 18, 24 days). Freshly isolated fascicles served as a positive tissue control (day 0). Devitalized fascicles were generated by three freeze-thaw cycles before further use and served as negative control. Fascicles were cultured in serum-free medium (high glucose Dulbecco's Modified Eagle's Medium (DMEM), 1% N2-supplement (v/v), 1% penicillin-streptomycin (v/v), 200 μM L-ascorbic acid phosphate magnesium salt n-hydrate) or serum-supplemented medium (high glucose DMEM, 10% fetal bovine serum (v/v), 1% penicillin-streptomycin (v/v), 1% non-essential amino acids (v/v), 200 μM L-ascorbic acid phosphate magnesium salt n-hydrate). Fascicles were maintained in a humidified atmosphere containing 5% CO_2 at either low oxygen partial pressure ($pO_2 = 3$ kPa) and low temperature (29 °C) or high oxygen partial pressure ($pO_2 = 20$ kPa) and temperature (37 °C). The fascicles in serum-supplemented medium were additionally cultured in intermediate conditions at high oxygen and low temperature or vice versa.

Medium was changed every sixth day. All compounds of the cell culture media were purchased from Sigma Aldrich, except for the ascorbic acid (Wako Chemicals) and the N2-supplement (Gibco). The Cantonal Veterinary office of Zürich ethically approved all animal experiments (permit number ZH265/14) and a total number of 40 mice were used.

Physiological tail tendon temperature of healthy mice was estimated by infrared-measurements of the cutaneous tail temperature in 40 animals (Infrared thermometer 153-IRB, Bioseb).

Biomechanical testing and analysis

Force-displacement data were recorded from N = 6 independent fascicles from different mice on a custom-made uniaxial stretch device as previously described [15]. In brief, fascicles were clamped, pre-loaded to 0.015 N (corresponding to 0% strain) and preconditioned to 1% strain with five stretch cycles. The tangential elastic-modulus was calculated in the linear part of the stress-strain curve (0.5−1% strain) of a single additional stretch cycle to 1% by fitting a linear slope (Matlab R2016a, Version 9.0.0.341360). The pre-load was reapplied after every cycle. Nominal stress was calculated based on the initial cross-sectional area. Cross-sectional area was determined from the diameter assuming a round specimen shape. Diameter was measured using automated evaluation of microscopic images (Matlab R2016a, Version 9.0.0.341360), which were recorded before the treatment at three different locations along the fascicle with a 20-fold magnification (Motic AE2000, Plan LWD 20x, WD 4.7).

Cell viability and ATP measurements

Dead cells in the fascicles were stained with Ethidium Homodimer-1 (2 μM, AS 83208, Anaspec) previous to 10% formalin fixation (HT5011, Sigma Aldrich). Subsequently, cell nuclei were stained with NucBlue reagent (1 drop/ml = ca. 10 μl, R37606, Thermo Fischer, Switzerland) and embedded in a 50% Glycerol:PBS solution. Z-stack fluorescent images were obtained in triplicates by using a spinning disc confocal microscope (iMic, FEI) equipped with a Hamamatsu Flash 4.0 sCMOS camera and a SOLE-6 Quad laser (Omicron) and using a 20× objective (Olympus, UPLSAPO, N.A. 0.75). Total number of imaged cells, percentage live cells (total cell number minus dead cells) and fascicle volume (N = 6, independent fascicles from different mice) were assessed by means of a custom microscopic image analysis tool (MATLAB, R2016a 9.00.34160). Number of cells was determined in a measurement depth of 60 μm (from surface) and the volume of the circular segment was calculated by measuring length and diameter of the total specimen z-projection.

ATP was assessed by using a luminescence based ATP detection assay according to the manufacturer's instructions (CellTiterGlo3D, G9681, Promega). ATP standards were prepared from a 10 mM stock solution (P1132, Promega). After ATP measurement the 20 mm long fascicle parts (N = 4 biological replicates, for each N two technical replicates were measured, two fascicles per animal) were frozen at −80 °C and subsequently digested at 56 °C overnight by Proteinase K (10 mM in Tris-HCl, 19133, Qiagen). To account for potentially differential cell proliferation rate between treatments all the ATP quantifications were normalized to DNA content in the same samples. The quantity of DNA in each digest was measured by fluorescent signal detection using the Quant-iT™ dsDNA High-Sensitivity Assay Kit (Q33232, Thermo Fisher) according to the manufacturer's protocol. Whole fascicles were cut to equally sized parts (20 mm), while one half was processed and measured directly after isolation (day 0) and the other half after the treatment (day 6 and 12). Luminescence and fluorescence were both recorded on a microplate reader (SpectraMAX Gemini XS).

Second harmonic generation imaging and transmission electron microscopy of tendon fascicles

Collagen was visualized by second harmonic generation (SHG) imaging of whole mount tissues on a multi-photon and confocal fluorescence microscope (Leica TCS SP8) equipped with photon-counting hybrid detectors and an ultrafast near infrared laser (Insight DS + Dual, Spectra Physics) using 25× magnification (HC IRAPO L 25x, NA 1.0), an excitation wavelength of 880 nm and a SHG-compatible fluorescence filter cube (440/20 & 483/32 with 455 SP). Cell nuclei were imaged from the same samples. All the samples were recorded at the same laser power

and gain control with a z-step size of 0.3 μm. After image acquisition 70 stacks were z-projected using ImageJ (Fiji, NIH Version 1.0).

For transmission electron microscopy whole mouse tail tendon fascicles were fixed in 2.5% glutaraldehyde (G5882, Sigma-Aldrich) in 0.1 M Cacodylat buffer (pH 7.2) for 20 min. To visualize the collagen fibrils, samples were contrasted with 1% uranyl acetate in water for 1 h. All samples were then dehydrated with graduated concentration of ethanol and propylene oxide. Specimens were infiltrated and embedded in Epon (polymerized at 60 °C for 48 h). Ultra-thin longitudinal and cross sections were cut with a diamond knife and mounted on uncoated grids. Samples were then imaged with a transmission electron microscope (TEM-FEI Tecnai G2 Spirit).

RNA sequencing

For each experimental group 16–20 fascicles were pooled after 6 days of culture. Each independent pool was created from a single mouse and represents one biological replicate (N). Fascicle pools (N = 3) were snap frozen in liquid nitrogen and pulverized in QIAzol lysis reagent (#79306, Qiagen) by cryogenic grinding (FreezerMill 6870, SPEX^{TM}SamplePrep). Tissue lysates were mixed with 1-bromo-3-chloropropane (B9673, Sigma-Aldrich) at a ratio of 1:4 and the RNA containing aqueous/organic phase was separated using 5Prime PhaseLock Gel Heavy (#2302830, LabForce). RNA was extracted by using the RNeasy micro Kit (74004, Qiagen). The quantity and quality of the isolated RNA was determined with a Qubit® (1.0) Fluorometer (Life Technologies, California, USA) and a Bioanalyzer 2100 (Agilent, Waldbronn, Germany). The TruSeq Stranded mRNA Sample Prep Kit (Illumina, Inc, California, USA) was used in the succeeding steps. Briefly, total RNA samples (100 ng) were poly-A selected and then reverse-transcribed into double-stranded cDNA with Actinomycin added during first-strand synthesis. The cDNA sample was fragmented, end-repaired and adenylated before ligation of TruSeq adapters. The adapters contain the index for multiplexing. Fragments containing TruSeq adapters on both ends were selectively enriched with RT-PCR. The quality and quantity of the enriched libraries were validated using Qubit® (1.0) Fluorometer and the Bioanalyzer 2100 (Agilent, Waldbronn, Germany). The product is a smear with an average fragment size of approximately 360 bp. The libraries were normalized to 10 nM in Tris-Cl 10 mM, pH8.5 with 0.1% Tween 20. The TruSeq SR Cluster Kit v4-cBot-HS (Illumina, Inc, California, USA) was used for cluster generation using 8 pM of pooled normalized libraries on the cBOT. Sequencing was performed on the Illumina HiSeq 4000 single end 125 bp using the TruSeq SBS Kit v4-HS (Illumina, Inc, California, USA).

RNA sequencing data analysis

Bioinformatic analysis was performed using the R package ezRun[1] within the data analysis framework SUSHI [43]. In details, the raw reads were quality checked using Fastqc[2] and FastQ Screen.[3] Quality controlled reads (adapter trimmed, first 5 and last 6 bases hard trimmed, minimum average quality Q10, minimum tail quality Q10, minimum read length 20 nt) were aligned to the reference genome (Ensembl GRCm38.p5) using the STAR aligner [44]. Expression counts were computed using featureCounts in the Bioconductor package Subread [45]. Differential expression analysis was performed using the DESeq2 package [46], where raw read counts were normalized using the quantile method, and differential expression was computed using the quasi-likelihood (QL) F-test.[4] Gene ontology (GO) enrichment analysis was performed using Bioconductor packages goseq [47] and GOStats [48]. Quality checkpoints [49], such as quality control of the alignment and count results, were implemented in ezRun and applied through out the analysis workflow to ensure correct data interpretation. Differentially expressed genes were considered at a p-value < 0.05 and a $|\text{fold change}| > 2$. Pathway analyses were performed using MetaCore database via GeneGo tool from Thomson Reuters[5] and the Kyoto Encyclopedia of Genes and Genomes (KEGG) database.

Detection of reactive oxygen species

To quantify the production of reactive oxygen species (ROS) tendon fascicles (N = 6, independent fascicles from different mice) were stained with 2′,7′-Dichlorofluorescin diacetate (DCFH-DA, D6883, Sigma Aldrich). DCFH-DA is a cell-permeable compound, which upon esterase cleavage may be oxidized intracellularly to produce the fluorescent dichlorofluorescein (DCF). Control fascicles and cultured fascicles were incubated for 30 min with 50 μM DCFH-DA in PBS at either 29 °C, 3 kPa pO_2 or 37 °C, 20 kPa pO_2 at day 0 and day 6 according to the previous culture. Immediately after incubation, fluorescence was recorded by acquiring z-stacks at steps of 1 μm through the whole fascicles depth at an excitation wavelength of 488 nm on the spinning disc confocal microscope setup as described above using a 10× objective (Olympus, UPLSAPO, N.A. 0.4). Quantification of fluorescent signal reflected from the tissue was evaluated by measuring cumulative mean intensity of z-projections using ImageJ (Fiji, NIH Version 1.0). Images were taken in triplicates.

Quantitative real-time polymerase chain reaction (RT-PCR)

RNA was extracted from N = 4 biological replicates (one N was created from a pool of fascicles from a single mouse) as described above but using the PureLink™ RNA Micro Scale Kit (#12183016, Invitrogen). cDNA was prepared by reverse transcribing 99 ng total RNA in a volume of 44 μl using the High-Capacity RNA-to-cDNA™ Kit (#4387406, Applied Biosystems). RT-PCR was carried out using 2 μl cDNA, 5 μl TaqMan Universal Master Mix,

1 https://github.com/uzh/ezRun.

2 http://www.bioinformatics.babraham.ac.uk/projects/fastqc/.

3 http://www.bioinformatics.babraham.ac.uk/projects/fastq_screen/.

4 https://bioconductor.org/packages/devel/bioc/manuals/DESeq2/man/DESeq2.pdf.

5 https://portal.genego.com/.

0.5 μl TaqMan Primer (Applied Biosystems) and 2.5 μl RNase free water. Samples were amplified in 40 cycles on a StepOnePlus™ thermocycler (Applied Biosystems) and reactions were run in technical duplicates. Following primers were used: Mm00442991_m1 (*Mmp9*), Mm01168399_m1 (*Mmp10*), Mm00439491_m1 (*Mmp13*), Mm01310506_m1 (*Ctsb*), Mm00515580_m1 (*Ctsc*), Mm00515586_m1 (*Ctsd*), Mm01255859_m1 (*Ctss*), Mm00517697_m1 (*Ctsz*). Relative gene expression was calculated by the comparative Ct method [50] by normalizing the data to the stable housekeeping gene Mm0129059_m1 (*Anxa5*) and to freshly isolated samples.

Inhibition experiments

Tendon fascicles (N = 7, independent fascicles from different mice) were cultured under degrading conditions (serum, 37 °C and 20 kPa pO_2) for 12 days. From the beginning of the incubation time medium was supplemented with the ROS inhibitor Tempol (4-hydroxy-2,2,6,6-tetramethylpiperidin-1-oxyl) (1 mM, 176141-1G, Sigma), the MMP inhibitor Ilomastat ((*R*)-*N*′-Hydroxy-*N*-[(S)-2-indol-3-yl-1-(methylcarbamoyl)ethyl]-2-isobutylsuccinamide) (25 μM, CC1010, Merck Millipore) or a combination of both. Tempol is a membrane-permeable superoxide dismutase mimetic that serves in the reaction of superoxide radical to yield hydrogen peroxide. Ilomastat is a broad-spectrum MMP inhibitor that interacts with the zinc ion in the active site of catalytic domain of the enzyme. Medium with DMSO (#472301, Sigma) was used as a control. Culture medium was changed after 6 days. Elastic modulus was measured at day 0 and day 12 and negative control fascicles were devitalized as described above.

Mass spectrometry-based proteomics

For terminal amine isotope labeling of substrates (TAILS) experiments, N = 5 biological replicates (one N represents an independent pool of fascicles from a single mouse) were snap frozen from 12 day cultures of mechanically intact and impaired fascicles. TAILS analysis, whereby protein N-termini were enriched, was performed according to the previously described protocol [51] except for using 10plex Tandem mass Tag™ labeling (TMT, #90110, Thermo Fisher) and adding the trypsin at a ratio of 1:20 (trypsin/protein ratio). Prior to protein denaturation and labeling, proteins of samples were extracted by pressure cycling technology (60 cycles of 45′000psi for 20 s, atmospheric pressure for 10 s, 33 °C) from ca. 4 mg tissue in a buffer containing 4 M Guanidine hydrochloride (Sigma-Aldrich), 250 mM HEPES (Sigma-Aldrich (pH 7.8)) and protease inhibitor cocktail (cOomplete EDTA-free, Roche) using a Barocycler 2320ETX (Pressure Biosciences Inc.) (Fig. 5A).

Secretomes of 18–22 equally sized and 12-days-cultured fascicles were collected for each of the two conditions in 2 ml serum-free and phenol red-free DMEM (#31053028, Gibco supplemented with 1% penicillin-streptomycin (v/v), 200 μM L-ascorbic acid phosphate magnesium salt n-hydrate and 1% GlutaMAX (v/v), A1286001, Gibco) during an exposure time of 48 h. Fascicles were thoroughly washed with PBS before secretome collection. Secretomes were supplemented with protease inhibitor cocktail (cOomplete EDTA-free, Roche) and concentrated ca. 40 times by centrifugal filtration (3 K Amicon Ultra, Merck Millipore, 14′000 g, 4 °C) and buffer was exchanged to 4 M Guanidine hydrochloride in 50 mM HEPES (pH 7.8). Subsequently, secretomes were reduced in tris(2-carboxyethyl)phosphine (200 mM, Sigma-Aldrich) and alkylated in chloroacetamide (400 mM, Sigma-Aldrich) for 30 min at room temperature and then digested by LysC (Lysyl endopeptidase, #125–05061, Wako, ratio LysC/protein 1:100) and trypsin (Trypsin Gold, V5280, Promega, ratio trypsin/protein 1:20) overnight. Desalting was performed according to the TAILS protocol [51].

PreTAILS, TAILS and secretome peptide mixtures were loaded onto an PepMap100C18 precolumn (75 μm × 2 cm, 3 μm, 100 Å, nanoViper, Thermo Scientific) and separated on a PepMap RSLC C18 analytical column (75 μm × 50 cm, 2 μm, 100 Å, nanoViper, Thermo Scientific) using an EASY-nLC™ 1000 liquid chromatography system (Thermo Scientific) coupled in line with a Q Exactive mass spectrometer (Thermo Scientific). Separation of 1 μg of peptide mixture was achieved by running a constant flow rate of 250 nL/min in 0.1% formic acid/99.9% water and a 140 min gradient from 10% to 95% (23% for 85 min, 38% for 30 min, 60% for 10 min, 95% for 15 min) elution buffer (80% acetonitrile, 0.1% formic acid, 19.9% water). A data-dependent acquisition (DDA) method operated under Xcalibur 3.1.66.10 was applied to record the spectra. For the preTAILS and TAILS samples the full scan MS spectra (300–1750 *m/z*) were acquired with a resolution of 70'000 after accumulation to a target value of 3e6. Higher-energy collisional dissociation (HCD) MS/MS spectra with fixed first mass of 120 *m/z* were recorded from the 10 most intense signals with a resolution of 35,000 applying an automatic gain control of 1e6 and a maximum injection time of 120 ms. Precursors were isolated using a window of 1.6 *m/z* and fragmented with a normalized collision energy (NCE) of 28%. Precursor ions with unassigned or single charge state were rejected and precursor masses already selected for MS/MS were excluded for further selection for 60s. Settings for the scan of the secretome peptide mixture were the same except for using a resolution of 17'500 for recording the MS/MS spectra, a maximum injection time of 60 ms, and a NCE of 25%.

Proteomics data analysis

Raw data files were analyzed using Proteome Discoverer™ 2.3 software (PD) searching the peak lists against a database collated in the UniProt reference proteome for the species *Mus musculus* (ID: 10090, entries: 17′005). Search parameters for the TAILS experiment were set according to the previously published protocol [51], treating preTAILS and TAILS samples as fractions. For protein-level analysis, quantifiable internal fully tryptic peptides and mature protein N-termini were annotated with help of TAILS-Annotator [52], extracted from PD peptide groups and their normalized, scaled abundances were summed up per corresponding protein. The resulting list was curated for protein FDR<0.01 based on PD protein analysis and proteins with significantly differential abundance between conditions determined applying limma moderated t-statistics with Bonferroni-Hochberg multiple testing correction in CARMAweb [53]. Similarly, quantifiable N-terminal peptides were extracted from the PD analysis, annotated using TopFIND [54] and analyzed for statistically differential abundance using CARMAweb

applying the same parameters as for proteins based on scaled abundances summed up per stripped peptide sequence. Volcano plots were generated using GraphPad Prism (GraphPad Software 8.0).

Raw data files of the secretome experiments were processed by PD using the label-free quantification algorithm Minora Feature Detector node and proteins tested for differential abundance between conditions applying limma moderated t-statistics using CARMAweb [53] on normalized scaled abundance values exported from PD.

Statistics

RStudio (Version 1.1.423, 2016, Boston, MA) was used for statistical tests and graph illustrations [55]. Mean values of elastic moduli were compared by one-way analysis of variance (ANOVA) followed by contrast analysis. Additionally, multiple linear regression analysis was used to assess the linear relationship between culture time-points, temperature, oxygen and serum as predictors for the response variable elastic modulus. Temperature, oxygen and serum were coded as 0 = 29 °C/3 kPa O_2/no serum and 1 = 37 °C/20 kPa O_2,/10% serum, respectively. Non-parametric data (percentage live cells, total cell number, ATP measurement, RT-PCR, DCFH-DA measurement) was analyzed by means of the Mann-Whitney *U* test to probe for differences between two treatment groups. Results were considered to be statistically significant with × at p-values < 0.05, ** <0.01 and *** <0.001. Further information on individual statistical tests is available in the respective figure legends.

Availability of data and material

The RNA-sequencing data from this publication have been deposited to the Annotare database (https://www.ebi.ac.uk/fg/annotare) and assigned the identifier E-MTAB-7832.

The mass spectrometry proteomics data have been deposited to the ProteomeXchange Consortium (http://proteomecentral.proteomexchange.org) via the PRIDE (PRoteomics IDentifications) partner repository [31] with the data set identifier PXD013635.

Author contributions

Study concept and design: SLW, FSP, US, JGS. Collection and/or assembly of data: SLW, UB, ABP, BN, LB. Data analysis: SLW, UB, CNH, UADK. Data interpretation and manuscript writing: SLW, UB, UADK, JGS.

Acknowledgment

We gratefully thank Max Hess and Lucien Segessemann for their important contribution and expertise in image analysis, Jonathan Ward, Susanne Freedrich, Kerstin Sacher and Gisela Kuhn (ETH Phenomics Center) for providing the research animals and their assistance in the animal facility. We thank Ursula Lüthi, José María Mateos and Andrés Käch (Center for Microscopy and Image Analysis, Zürich) for TEM microscopy, Lilian Hartmann and Olivier Leupin for technical assistance in the RNA isolation procedure and Jelena Kühn Georgijevic and Weihong Li (Functional Genomics Center, Zürich) for their support on RNA sequencing data. The authors further gratefully acknowledge the valuable support of Elizabeta Madzharova during the TAILS procedure and Tobias Götschi for the help on statistical data analysis. This work has been funded by ETH (Grant 12-13-2), the Vontobel Foundation, the Swiss National Science Foundation (P1EZP3-181729) and a Novo Nordisk Foundation Young Investigator Award (NNF16OC0020670).

Appendix A. Supplementary data

Supplementary data to this article can be found online at https://doi.org/10.1016/j.matbio.2019.12.003.

Received 24 September 2019;
Received in revised form 17 December 2019;
Accepted 17 December 2019
Available online 07 January 2020

Keywords:
Tendon;
Explant;
Reactive oxygen species (ROS);
Proteases;
Tissue model

Abbreviations used:
DEG, Differentially expressed gene; GO, Gene ontology; HiO_2HiT+, High oxygen (20 kPa), high temperature (37 °C), with 10% serum; LoO_2LoT+, Low oxygen (3 kPa), low temperature (29 °C), with 10% serum; ROS, Reactive oxygen species; TMT-TAILS, Tandem Mass Tag™-Terminal amine isotopic labeling of substrates.

References

[1] A.H. Lee, D.M. Elliott, Comparative multi-scale hierarchical structure of the tail, plantaris, and Achilles tendons in the rat, J. Anat. 234 (2) (2019) 252–262.
[2] M. O'Brien, Structure and metabolism of tendons, Scand. J. Med. Sci. Sport. 7 (2) (1997) 55–61.
[3] C.N. Riggin, T.R. Morris, L.J. Soslowsky, Tendinopathy II: Etiology, Pathology, and Healing of Tendon Injury and Disease, Tendon Regeneration, Elsevier, 2015, pp. 149–183.

[4] A. McCormick, J. Charlton, D. Fleming, Assessing health needs in primary care. Morbidity study from general practice provides another source of information, BMJ, Br. Med. J. 310 (6993) (1995) 1534.
[5] Y. Xu, G.A. Murrell, The basic science of tendinopathy, Clin. Orthop. Relat. Res. 466 (7) (2008) 1528–1538.
[6] R.V. Iozzo, M.A. Gubbiotti, Extracellular matrix: the driving force of mammalian diseases, Matrix Biol. 71–72 (2018) 1–9.
[7] S.P. Magnusson, H. Langberg, M. Kjaer, The pathogenesis of tendinopathy: balancing the response to loading, Nat. Rev. Rheumatol. 6 (5) (2010) 262–268.
[8] E.L. Abreu, D. Leigh, K.A. Derwin, Effect of altered mechanical load conditions on the structure and function of cultured tendon fascicles, J. Orthop. Res. : Off. Pub. Orthop. Res. Soc. 26 (3) (2008) 364–373.
[9] H. Tempfer, A. Traweger, Tendon vasculature in health and disease, Front. Physiol. 6 (2015) 330.
[10] A. Carreau, B. El Hafny-Rahbi, A. Matejuk, C. Grillon, C. Kieda, Why is the partial oxygen pressure of human tissues a crucial parameter? Small molecules and hypoxia, J. Cell Mol. Med. 15 (6) (2011) 1239–1253.
[11] K. Kubo, T. Ikebukuro, N. Tsunoda, H. Kanehisa, Non-invasive measures of blood volume and oxygen saturation of human Achilles tendon by red laser lights, Acta Physiol. 193 (3) (2008) 257–264.
[12] S.P. Magnusson, K.M. Heinemeier, M. Kjaer, Collagen Homeostasis and Metabolism, Metabolic Influences on Risk for Tendon Disorders, Springer, 2016, pp. 11–25.
[13] J.G. Snedeker, J. Foolen, Tendon injury and repair - a perspective on the basic mechanisms of tendon disease and future clinical therapy, Acta Biomater. 63 (2017) 8–36.
[14] M. Järvinen, L. Józsa, P. Kannus, T.L.N. Järvinen, M. Kvist, W. Leadbetter, Histopathological findings in chronic tendon disorders, Scand. J. Med. Sci. Sport. 7 (2) (1997) 86–95.
[15] S.L. Wunderli, J. Widmer, N. Amrein, J. Foolen, U. Silvan, O. Leupin, J.G. Snedeker, Minimal mechanical load and tissue culture conditions preserve native cell phenotype and morphology in tendon-a novel ex vivo mouse explant model, J. Orthop. Res. : Off. Pub. Orthop. Res. Soc. 36 (5) (2018) 1383–1390.
[16] G.F. Fasciglione, S. Marini, S. D'Alessio, V. Politi, M. Coletta, pH-and temperature-dependence of functional modulation in metalloproteinases. A comparison between neutrophil collagenase and gelatinases A and B, Biophys. J. 79 (4) (2000) 2138–2149.
[17] X. Shao, I.N. Taha, K.R. Clauser, Y.T. Gao, A. Naba, MatrisomeDB: the ECM-protein knowledge database, Nucleic Acids Res. 48 (2020) 1136–1144.
[18] J.C. Hewlett, J.A. Kropski, T.S. Blackwell, Idiopathic pulmonary fibrosis: epithelial-mesenchymal interactions and emerging therapeutic targets, Matrix Biol. 71–72 (2018) 112–127.
[19] P. Cousineau-Pelletier, E. Langelier, Relative contributions of mechanical degradation, enzymatic degradation, and repair of the extracellular matrix on the response of tendons when subjected to under- and over- mechanical stimulations in vitro, J. Orthop. Res. : Off. Pub. Orthop. Res. Soc. 28 (2) (2010) 204–210.
[20] S. Arnoczky, T. Tian, M. Lavignano, K. Gardner, Ex vivo static tensile loading inhibits MMP-1 expression in rat tail tendon cells through a cytoskeletally based mechanotransduction mechanism, J. Orthop. Res. 22 (2) (2004) 328–333.
[21] T. Stauber, U. Blache, J.G. Snedeker, Tendon tissue microdamage and the limits of intrinsic repair, Matrix Biol. (2019), https://doi.org/10.1016/j.matbio.2019.07.008.
[22] N.A. Afratis, M. Selman, A. Pardo, I. Sagi, Emerging insights into the role of matrix metalloproteases as therapeutic targets in fibrosis, Matrix Biol. 68–69 (2018) 167–179.
[23] S.S. Apte, W.C. Parks, Metalloproteinases: a parade of functions in matrix biology and an outlook for the future, Matrix Biol. : J. Int. Soc. Matrix Biol. 44–46 (2015) 1–6.
[24] J.E. Murphy-Ullrich, M.J. Suto, Thrombospondin-1 regulation of latent TGF-beta activation: a therapeutic target for fibrotic disease, Matrix Biol. 68–69 (2018) 28–43.
[25] F. Wang, G.A. Murrell, M.X. Wang, Oxidative stress-induced c-Jun N-terminal kinase (JNK) activation in tendon cells upregulates MMP1 mRNA and protein expression, J. Orthop. Res. : Off. Pub. Orthop. Res. Soc. 25 (3) (2007) 378–389.
[26] B.K. Pedersen, L. Hoffman-Goetz, Exercise and the immune system: regulation, integration, and adaptation, Physiol. Rev. 80 (3) (2000) 1055–1081.
[27] G. Csányi, M. Yao, A.I. Rodríguez, I.A. Ghouleh, M. Sharifi-Sanjani, G. Frazziano, X. Huang, E.E. Kelley, J.S. Isenberg, P.J. Pagano, Thrombospondin-1 regulates blood flow via CD47 receptor–mediated activation of NADPH oxidase 1, Arterioscler. Thromb. Vasc. Biol. 32 (12) (2012) 2966–2973.
[28] K. Bedard, K.-H. Krause, The NOX family of ROS-generating NADPH oxidases: physiology and pathophysiology, Physiol. Rev. 87 (1) (2007) 245–313.
[29] S.G. Dakin, F.O. Martinez, C. Yapp, G. Wells, U. Oppermann, B.J. Dean, R.D. Smith, K. Wheway, B. Watkins, L. Roche, Inflammation activation and resolution in human tendon disease, Sci. Transl. Med. 7 (311) (2015), 311ra173-311ra173.
[30] X. Zhao, P. Psarianos, L.S. Ghoraie, K. Yip, D. Goldstein, R. Gilbert, I. Witterick, H. Pang, A. Hussain, J.H. Lee, J. Williams, S.V. Bratman, L. Ailles, B. Haibe-Kains, F.-F. Liu, Metabolic regulation of dermal fibroblasts contributes to skin extracellular matrix homeostasis and fibrosis, Nat. Metab. 1 (1) (2019) 147–157.
[31] C. Tu, C.F. Ortega-Cava, G. Chen, N.D. Fernandes, D. Cavallo-Medved, B.F. Sloane, V. Band, H. Band, Lysosomal cathepsin B participates in the podosome-mediated extracellular matrix degradation and invasion via secreted lysosomes in v-Src fibroblasts, Cancer Res. 68 (22) (2008) 9147–9156.
[32] W.C. Parks, C.L. Wilson, Y.S. Lopez-Boado, Matrix metalloproteinases as modulators of inflammation and innate immunity, Nat. Rev. Immunol. 4 (8) (2004) 617–629.
[33] H. Kono, K.L. Rock, How dying cells alert the immune system to danger, Nat. Rev. Immunol. 8 (4) (2008) 279–289.
[34] C. Settembre, L. Cinque, R. Bartolomeo, C. Di Malta, C. De Leonibus, A. Forrester, Defective collagen proteostasis and matrix formation in the pathogenesis of lysosomal storage disorders, Matrix Biol. 71–72 (2018) 283–293.
[35] S. Burgdorf, M. Embgenbroich, Current concepts of antigen cross-presentation, Front. Immunol. 9 (2018) 1643.
[36] M. Hansen, M. Kjaer, Sex hormones and tendon, Adv. Exp. Med. Biol. 920 (2016) 139–149.
[37] D.C. Sarver, Y.A. Kharaz, K.B. Sugg, J.P. Gumucio, E. Comerford, C.L. Mendias, Sex differences in tendon structure and function, J. Orthop. Res.: Off. Pub. Orthop. Res. Soc. 35 (10) (2017) 2117–2126.
[38] G.C. Jones, A.N. Corps, C.J. Pennington, I.M. Clark, D.R. Edwards, M.M. Bradley, B.L. Hazleman, G.P. Riley, Expression profiling of metalloproteinases and tissue inhibitors

of metalloproteinases in normal and degenerate human achilles tendon, Arthritis Rheum. 54 (3) (2006) 832–842.
[39] S. Minkwitz, A. Schmock, A. Kurtoglu, S. Tsitsilonis, S. Manegold, B. Wildemann, F. Klatte-Schulz, Time-Dependent Alterations of MMPs, TIMPs and tendon structure in human achilles tendons after acute rupture, Int. J. Mol. Sci. 18 (10) (2017).
[40] A.N. Corps, G.C. Jones, R.L. Harrall, V.A. Curry, B.L. Hazleman, G.P. Riley, The regulation of aggrecanase ADAMTS-4 expression in human Achilles tendon and tendon-derived cells, Matrix biology, J. Int. Soc. Matrix Biol. 27 (5) (2008) 393–401.
[41] S.P. Seto, A.N. Parks, Y. Qiu, L.J. Soslowsky, S. Karas, M.O. Platt, J.S. Temenoff, Cathepsins in Rotator Cuff Tendinopathy: identification in human chronic tears and temporal induction in a rat model, Ann. Biomed. Eng. 43 (9) (2015) 2036–2046.
[42] M. Mack, Inflammation and fibrosis, Matrix Biol. 68–69 (2018) 106–121.
[43] M. Hatakeyama, L. Opitz, G. Russo, W. Qi, R. Schlapbach, H. Rehrauer, SUSHI: an exquisite recipe for fully documented, reproducible and reusable NGS data analysis, BMC Bioinf. 17 (1) (2016) 228.
[44] A. Dobin, C.A. Davis, F. Schlesinger, J. Drenkow, C. Zaleski, S. Jha, P. Batut, M. Chaisson, T.R. Gingeras, STAR: ultrafast universal RNA-seq aligner, Bioinformatics 29 (1) (2013) 15–21.
[45] Y. Liao, G.K. Smyth, W. Shi, featureCounts: an efficient general purpose program for assigning sequence reads to genomic features, Bioinformatics 30 (7) (2013) 923–930.
[46] M.I. Love, W. Huber, S. Anders, Moderated estimation of fold change and dispersion for RNA-seq data with DESeq2, Genome Biol. 15 (12) (2014) 550.
[47] M.D. Young, M.J. Wakefield, G.K. Smyth, A. Oshlack, Gene ontology analysis for RNA-seq: accounting for selection bias, Genome Biol. 11 (2) (2010) R14.
[48] S. Falcon, R. Gentleman, Using GOstats to test gene lists for GO term association, Bioinformatics 23 (2) (2007) 257–258.
[49] A. Conesa, P. Madrigal, S. Tarazona, D. Gomez-Cabrero, A. Cervera, A. McPherson, M.W. Szczesniak, D.J. Gaffney, L.L. Elo, X. Zhang, A. Mortazavi, A survey of best practices for RNA-seq data analysis, Genome Biol. 17 (2016) 13.
[50] T.D. Schmittgen, K.J. Livak, Analyzing real-time PCR data by the comparative C(T) method, Nat. Protoc. 3 (6) (2008) 1101–1108.
[51] E. Madzharova, F. Sabino, U. auf dem Keller, Exploring Extracellular Matrix Degradomes by TMT-TAILS N-Terminomics, Collagen, Springer, 2019, pp. 115–126.
[52] O. Kleifeld, A. Doucet, A. Prudova, U. auf dem Keller, M. Gioia, J.N. Kizhakkedathu, C.M. Overall, Identifying and quantifying proteolytic events and the natural N terminome by terminal amine isotopic labeling of substrates, Nat. Protoc. 6 (10) (2011) 1578–1611.
[53] J. Rainer, F. Sanchez-Cabo, G. Stocker, A. Sturn, Z. Trajanoski, CARMAweb: comprehensive R-and bioconductor-based web service for microarray data analysis, Nucleic Acids Res. 34 (suppl_2) (2006) W498–W503.
[54] N. Fortelny, S. Yang, P. Pavlidis, P.F. Lange, C.M. Overall, Proteome TopFIND 3.0 with TopFINDer and PathFINDer: database and analysis tools for the association of protein termini to pre- and post-translational events, Nucleic Acids Res. 43 (Database issue) (2015) D290–D297.
[55] R Core Team, R: A Language and Environment for Statistical Computing, R Foundation for Statistical Computing, Vienna, Austria, 2013.